Rolling Process Pelletizer Design for Bio-fertilizer Production

O. M. Abasili, U. C. Okonkwo*

Department of Mechanical Engineering, Faculty of Engineering, Nnamdi Azikiwe University, Awka, Nigeria

P A P E R I N F O	*A B S T R A C T*
	Rolling process pelletizer which provides more efficient pelletizing technique that eases bio-fertilizers production had been designed. The designed mechanisms were centered on the dynamics of the machine components that consist mainly of links and joints. Tensions and loads were determined by following the force balance equations. Bearings were selected from the SKF bearing catalogue by considering their positions, evaluation of the demands of the failure theories alongside with the dynamic load carrying capacities. Stability test was conducted on conveyor/mixing shaft of mass 11.2561kg and density 8000kg/m^3 by fixing one end and applying pressure of 1.061×10^{-3}N/mm^2 towards the other end in line with demands of distortion energy theory. Frame stability test was also conducted by applying beam mesh that generated 354 nodes and 334 elements. Tension of 205.2N and 126.5N were calculated at the pulley. Various loads and moments acting on different shafts were determined and represented diagrammatically. Von mises stress of 1.847E+00N/mm^2 on conveyor shaft and upper bound axial and bending stress of 2.759E+06N/m^2 on the frame that was below material's yield strength of 2.068E+08N/m^2 based on the result of simulation test indicated stability of the design. The design is expected to function as well in similar production areas.

NOMENCLATURE

r	Radius of the material (mm)	Z	Module of gear
h	Vertical height (mm)	C_d	Center to center distance for gears (mm)
L	Length of material (mm)	p	Circular pitch (mm)
T_q	Torque (Nmm)	F_R	Radial component of gear force (N)
P_T	Total tension (N)	b_L	Bearing life (million revs)
F_T	Tangential component of force (N)	D_L	Dynamic load (N)
C	Center to center distance for pulleys (mm)	V	Velocity of the belt (m/s)
P	Tension (N)	R	Normal reaction (N)
dP	Change in tension (N)	**Subscripts**	
m	Mass of one meter length of belt (kg/m)	p	Pinion
d	Shaft diameter (mm)	g	Gear
N	Revolutionary speed (rpm)	1, 2, 3	Pulley 1, 2 and 3
A	Area (mm^2)	**Greek Symbols**	
S_r	Speed ratio	$\emptyset$	Pressure angle (degree)
b_{Lh}	Bearing life (hours)	π	Pi number (assumed 3.142)
E_L	Equivalent load (N)	$d\gamma$	Angle subtended by belt element (degree)
k	Ball bearing factor = 3	α	Wrap angle (degree)
R_F	Resultant force (N)	φ	Belt angle (degree)
n	Number of teeth	ω	Angular velocity of the pulley (rad/s)
		σ	Maximum stress (N/mm^2)

Corresponding Author Email: cu.okonkwo@unizik.edu.ng

(U.C.Okonkwo)

INTRODUCTION

Bio-fertilizers production provided a very big relief to the challenges imposed by uncontrolled usage of the conventional chemical fertilizers [1-3]. Bio-fertilizers has various beneficial attributes to agricultural productivities along with its eco-friendliness, cost effectiveness and self- replenishing potentials [4-6]. Benefits of bio-fertilizers usage to organic farming could not be over emphasized. However, poor patronization of the finished product had posed a great challenge to the bio-fertilizers production process [7, 8]. Prolonged usage of conventional chemical fertilizers had etched the shape of pellets as the expected shape of fertilizers in the mind of the targeted farmers. Inability to convince farmers towards diverting to the improved technology dwindled the patronage and thus slowed down the production rate. Invariably, it could be depicted that bio-fertilizers producers pay more attention to the formulation of the bioinoculants and pay less attention to its appearance.

In line with the observations, many researchers had struggled to tackle the stated challenges and their efforts are quite appreciated. Oduntan et al. [9], Aremu et al. [10], Daniyan et al. [11], Daniyan and Akhere [12] and Pocius et al. [13] were among the reviewed researchers that made reasonable efforts towards ameliorating the situation although in contrast to full expectations of the farmers, their products formed irregular shapes as their pelletizing technology was based solely on extrusion process.

Efforts directed towards proffering a lasting solution to the challenges triggered the present study. Rolling process pelletizer design was presented in this study. Simplicity of the design is expected to ease the repair and maintenance. Various stages of the expected design are well delineated hereafter in this paper.

MATERIAL AND METHODS

Design principle and consideration for the rolling process pelletizer

The design is purely based on the dynamics of the machine components like the motor, belt, shaft, screw conveyor/mixer, rotary barrel and rolling process pelletizer. Then, circular motion of the listed components alongside with the gravitational motion of the feed stock, formed the basis of the machine operation. Electric motor in the design, transmit rotary motions to the driven shafts through the belt pulley arrangement. The success of the arrangement was through the centripetal and centrifugal forces that were associated with the circular motion. The desired result was obtained once the feed stock passed through the pelletizer and the required pellet obtained as the end product.

Design calculation of inlet hopper

The hopper was designed such that it assumed the shape of a shelled frustum of a square-based pyramid. Considering the expected throughput capacity of $10872640mm^3$, in line with economic considerations of the driving mechanisms, dimensions of the square-based of the frustum are 300mm in length and 300mm in width. The vertical height was 300mm and it was inclined at angle 60˚ so as to enable faster slip of the feedstock to the conveyor channel. Consider the sketch in Figure 1.

Applying Pythagoras theorem to determine the length of the diagonal of the base of the big pyramid $abcdi$.

$$|bd| = \sqrt{|bc|^2 + |cd|^2} = 424mm$$

$$|aj| = \frac{|bd|}{2} = 212mm$$

From tangent rule, $|jk| + |ki| = |aj|tan\emptyset = 367.2mm$

$$\therefore |ki| = 67.2mm$$

Applying Pythagoras theorem to triangle aji

$$|ai| = \sqrt{|aj|^2 + |ji|^2} = 474.2mm$$

Similarly, applying Pythagoras theorem to triangle eki, we have:

$$|ei| = \sqrt{|ek|^2 + |ki|^2} = 87.9mm$$

Therefore, the slant height of the hopper is then;

$$|ae| = |ai| - |ei| = 386.3mm$$

$volume\ of\ the\ hopper$
$$= volume\ of\ the\ big\ pyramid\ abcdi$$
$$- volume\ of\ the\ small\ pyramid\ efghi$$
$$= 10872640mm^3$$

Design of the fixed part of the conveyor/mixing inlet channel

$$The\ volume\ of\ the\ cylindrical\ shape = \pi r^2 h$$
$$= 603185.79mm^3$$

Design of belt and pulley

Figure 2 shows a belt drive traversing two pulley. The smaller pulley was connected to the motor spindle while
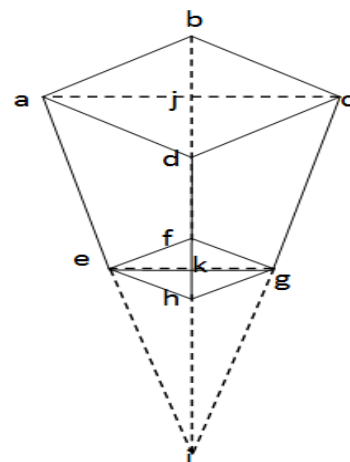

Figure 1. Pyramidal shape that described the hopper

the bigger pulley was connected to a driven shaft with the intention of reducing the angular speed.

Following the derivations and analysis of Vijayaraghavan and Vishnupriyan [14], Kolgiri Engineer's edge[1], Okoli and Okonkwo [15], the total length of the v-belt from Equation (1) becomes:

$$L = 2C + \pi\left(\frac{d_2 - d_1}{2}\right) + \frac{(d_2 - d_1)^2}{4C} = 638.43mm \qquad (1)$$

A case of another v-belt traversing three pulleys, as shown in the sketch of Figure 3.

The length of that type of V-belt was similarly given as Equation (2) by Evans[2] and Engineers edge [16] as:

$$L = C_{12} + C_{23} + C_{31} + \frac{1}{2}\left[\frac{\left(\frac{d_2-d_1}{2}\right)^2}{C_{12}} + \frac{\left(\frac{d_3-d_1}{2}\right)^2}{C_{31}} + \right.$$

$$\left.\frac{\left(\frac{d_3-d_2}{2}\right)^2}{C_{23}}\right] + \pi\left(\frac{d_1}{2} + \frac{d_2}{2} + \frac{d_3}{3}\right) - \left(\alpha_1\frac{d_1}{2} + \alpha_2\frac{d_2}{2} + \right. \qquad (2)$$

$$\left.\alpha_3\frac{d_3}{3}\right) = 442.29mm$$

Determination of Tension on the V-belt
The analysis of the forces acting on the element of V-belt that were represented in Figures 4 and 5.

In line with the works of Vijayaraghavan and Vishnupriyan [14], Kolgiri and Engineers edge [16] in analyzing the forces while they are in equilibrium;

$$(P + dP)sin\left(\frac{1}{2}d\gamma\right) + PSin\left(\frac{1}{2}d\gamma\right) - mV^2d\gamma - dRsin\left(\frac{1}{2}\varphi\right) = 0$$

Making the necessary substitutions and factorizations, Therefore, power transmitted is shown in Equation (3).

$$kW = \frac{(P_1 - P_2)V}{1000} \qquad (3)$$

Furthermore, in line with the works of Kolgiri, angular velocity of the pulley was in Equation (4).

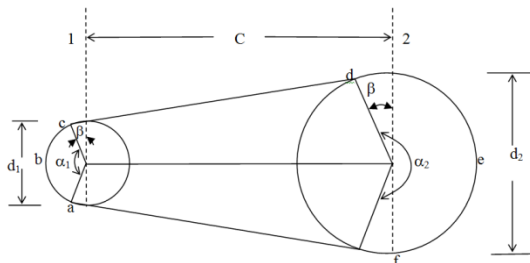$$\omega = \frac{2\pi N}{60} \; and \; V = r\omega = \frac{\pi dN}{60} \qquad (4)$$

Figure 2. Sketch of belt drive traversing two pulley
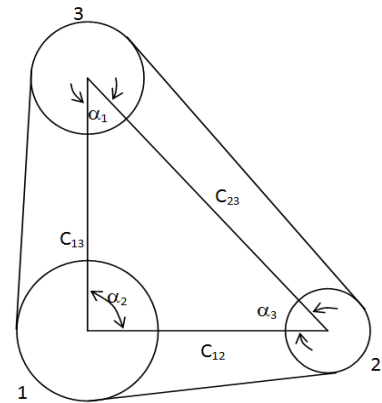
Figure 3. Sketch of V-belt traversing three pulleys

Velocity ratio between two pulley transmitting torque was presented in Equation (5).

$$\frac{\omega_1}{\omega_2} = \frac{d_2}{d_1} \qquad (5)$$

Also, from the works of Vijayaraghan and Vishnupriyan [14], tension on the tight side of the belt could equally be calculated with the formula in Equation (6).

$$P_1 = \sigma A \qquad (6)$$

where σ = maximum stress in the belt considered 2.25 N/mm^2. Calculation of the area of the belt A, from Figure 6 is in Equation (7).

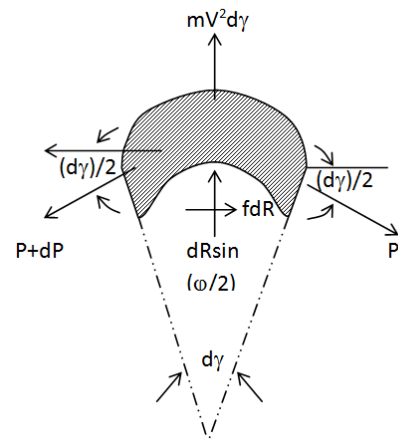$$A = \frac{1}{2}(|AB| + |GE|) \times |AD| = 91.2mm^2 \qquad (7)$$

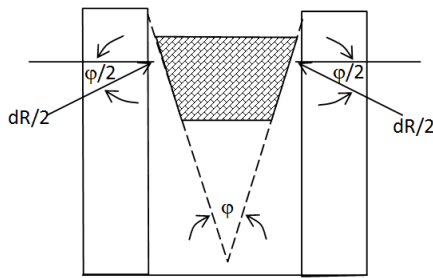**Figure 4.** Free body diagram showing forces acting on a v-belt element

[1]https://slideshare.net/sgkolgiri/unit-2-design-of-shaft

[2]https://theengineeringmindset.com/pulley-belt-calculations

Figure 5. Free body diagram showing forces acting on v-belt element in a pulley section

Spur gear design method

Spur gears that were used at different sections of the design were basically calculated in line with the works of Engineers edge [17], Kohara gear industry co.[1], Kolgiri and Vijayaraghavan and Vishnupriyan [14], the ratio of the speed of the pinion to the speed of the gear is Equation (8).

$$S_r = \frac{\omega_p}{\omega_g} = \frac{n_g}{n_p} \tag{8}$$

Pitch calculation $p = \frac{\pi d}{n} = \pi Z$. Then, center to center distance between two meshing gear is given in Equation (9) as:

$$C_d = \frac{1}{2}(d_p + d_g) = \frac{1}{2}(Zn_p + Zn_g)$$

$$C_d = \frac{Z(n_p + n_g)}{2} \tag{9}$$

Analysis of gear forces

The arrow in the Figure 7 indicated the direction of rotation of the mating gears which are in the opposite directions, viz: clockwise and anticlockwise. The sketch of the force analysis was indicated in the diagram of Figure 7.

Analyzing the forces in Figure 7, following the gear force analyses in the works of; Kolgiri and Engineers edge [17], the relationships in Equation (10) were obtained.

$$Power\ (kW) = \frac{2\pi N_{rpm} T_q}{60x1000x1000} \tag{10}$$

$$T_q = \frac{60x1000x1000xPower(kW)}{2\pi N_{rpm}}$$

Shafts design method

The various shafts used in the design were designed according to the design pattern of Kovacevic [18] and Kolgiri, in which the vertical loads and the horizontal

---

loads acting on each shaft were determined, followed by determination of the shear forces and bending moments. The shaft diameters will then be determined by considering the failure theories. The general process involved are elucidated as follows:

Determination of loads acting on the shaft

The loads acting on the shaft could be divided into vertical and horizontal loads. In a situation where the load acting on the shaft is due to belt and pulley arrangement; it could be determined through the Equations (11) and (12).

$$P_1 = \sigma A \tag{11}$$

$$P_2 = P_1 - \left(\frac{Power \times 1000}{V}\right)$$

Total load acting on the shaft at a point:

$$P_T = P_1 + P_2 \tag{12}$$

When the shaft is transmitting motion through gearing arrangements, Equations (13) and (14) was applied.

Torque, $T_q = \frac{60 \times 1000 \times 1000 \times Power\ (kW)}{2\pi N_{rpm}}$
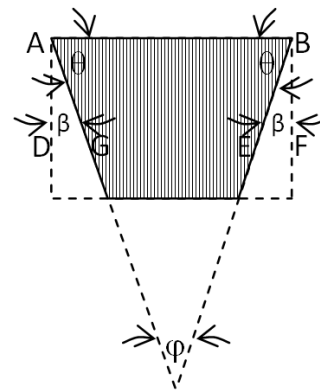
Tangential force,

$$F_T = \frac{2T_q}{d} \tag{13}$$
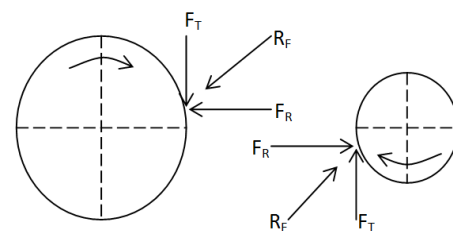

Figure 6. Sketch of the sectional area of the v-belt

Figure 7. Forces acting on mating

---

[1]https://khkgears.net/new/gear_knowledge/gear_technical_reference/calculation_gear_dimensions.html

Radial force,

$$F_R = F_T tan\emptyset \qquad (14)$$

Determination of reactions at the bearings

This is done by considering the force balance equation to obtain one equation, that is:

$$\sum Upward\ force = \sum Downward\ force$$

Then taking moment at one reaction point to obtain second equation, solve simultaneously and make necessary substitutions to determine the reactions.

Determination of bending moments

Bending moments could be determined by taking moment at the required points. The resultant bending moments are obtained through Pythagoras theory.

Determination of shaft diameter

This is done by considering the fulfilments of the requirements of the failure theories, viz; Coulomb, Tresca and Von Mises theories. Computation procedure were well presented by; Okoli et al.[15], Huajian [19], Burns [20], Atikpakpa [21], Kolgiri, Sengupta [22] and Atiyah [23].

Bearings design method

In doing this, Vijayaraghavan and Vishnupriyan [14], Kolgiri and SKF Group [24] described the relationship between life in working hours b_{Lh} and life in millions of revolutions b_L as presented in Equation (15):

$$b_L = \frac{60 \times N_{rpm} \times b_{Lh}}{10^6} \qquad (15)$$

The bearing life hour for gear and belt drive motor arrangement for at least eight hours' service per day was selected in line with Vijayaraghavan and Vishnupriyan[14], Kolgiri and SKF Group[24] as 12000 hours. After all the necessary substitutions, b_L was calculated. Then the equivalent loadE_L was calculated as the resultant load in each bearing.

Therefore, the dynamic load carrying capacity of the bearings that determined the number of revolutions which the bearing could run before the first evidence of fatigue crack, that was termed bearing life (SKF Group [24] ; Kolgiri), Okonkwo, et. al. [25] was then calculated as follows;

Dynamic load on the bearing at a Point D is obtained from Equation (16).

$$D_L = E_L \times b_L^{\frac{1}{k}} \times Load\ factor \qquad (16)$$

Simulation method on conveyor/mixing shaft

As 0.4 kg of feed stock is expected to be conveyed through the conveyor channel at a time, it is expected to impact 4N load on the conveyor/mixing shaft as well as the pressure value of 1.06×10^{-3} N/mm². The shaft is made

up of AISI 304 material of 11.2561kg in mass and 8000kg/m³ in density. The simulation was done with solid works 2020 software by fixing the end closer to the inlet hopper and applying the pressure of 1.06×10^{-3} N/mm²on the shaft while considering the demands of the Distortion energy theory.

Frame stability test

Frame was discretized into links and joints. A total of 12 joints out of the calculated 33 valid joints that linked to the base of the frame were fixed. The frame was then subjected to the weight of the other components of the machine that summed up to 397.1N, hence on compressive load. The weight was directed mainly to the frame link that supported the machine components while the reactions were observed and recorded.

RESULTS AND DISCUSSION

The entire calculations involving the determination of the shear forces, horizontal loads, vertical loads, horizontal bending moments, vertical bending moments and resultant bending moment on the various shafts were represented diagrammatically in Figures 8 to 12.
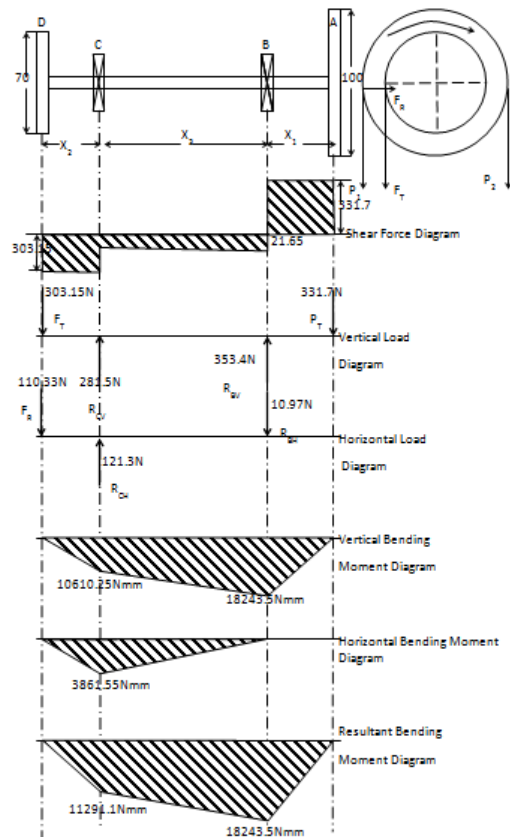

Figure 8. Sketch of load, stress and bending moments on the rotary barrel driving shaft
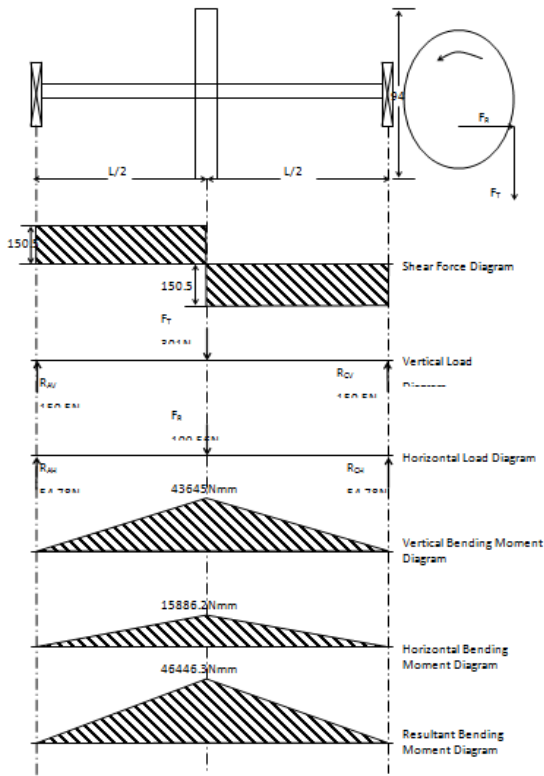
Figure 9. Sketch of load, stress and bending moments on the rotary barrel driven shaft
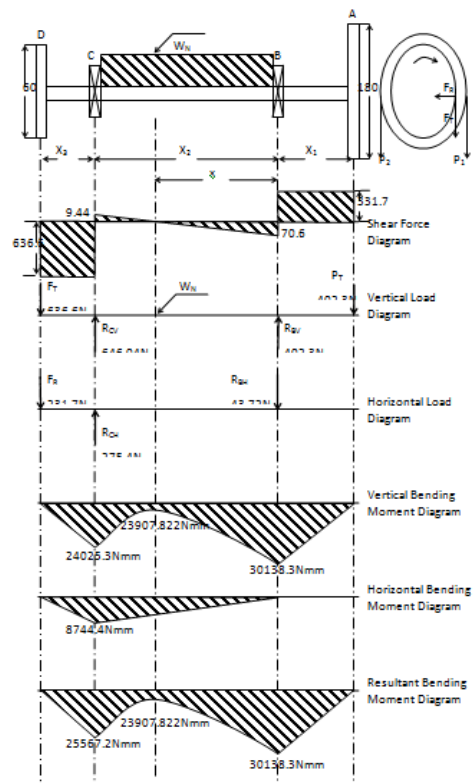

Figure 11. Sketch of load, stress and bending moment of pelletizer driving shaft
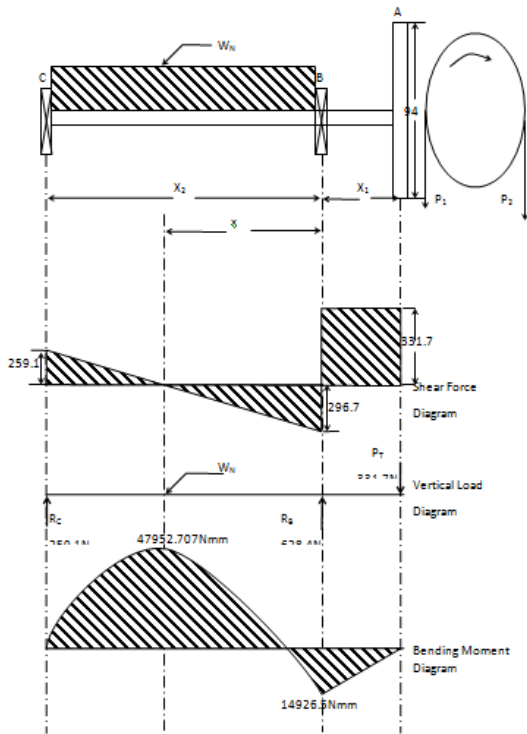

Figure 10. Sketch of load, stress and bending moment on conveyor/mixing shaft
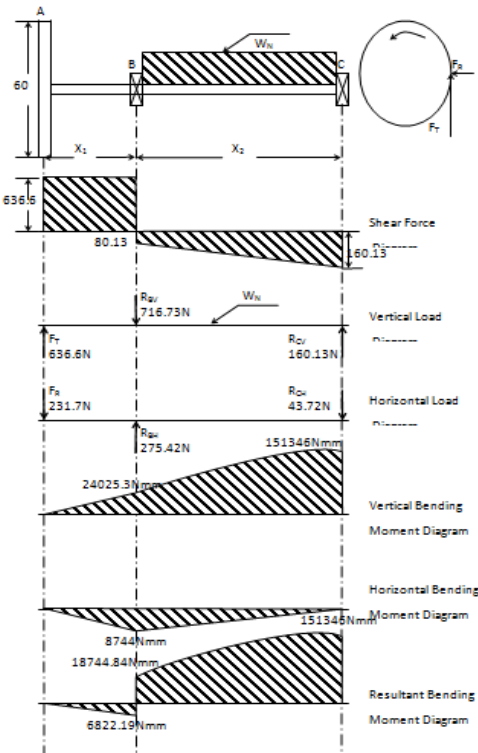

Figure 12. Sketch of loads, stress and bending moment for pelletizer driven shaft

The shear force diagrams showed the line of action of the various force while the bending moment diagram displays the deflection or resultant effects of the impact of those forces. Based on the shaft diameter of 10mm and the calculated dynamic loads in Figure 8, the bearing selection was obtained from manufacturer's catalogue designated to SKF Group [24]. The bearing selected for points B and C in Figure 8, is the single row deep groove ball bearing number: 6300 with inner diameter 10mm outer diameter 35mm, axial width 11mm, dynamic load carrying capacity of 8060N and static load carrying capacity of 3750N. Similarly, Considering the external diameter of the rotary barrel in Figure 9, as inner diameter of the expected cylindrical bearing, the calculated dynamic loads and the availability at the manufacturer's catalogue of SKF Group [24], the cylindrical roller bearing number: $NU1016$ with inner diameter 80mm, outer diameter 125mm, axial width 22mm, dynamic load carrying capacity 64.4kN, static load carrying capacity 78kN and fatigue load limit of 9.8kN. Likewise, Considering the selected shaft diameter of 15mm, the various dynamic loads computed Figure 10, the bearing selection was equally obtained from the manufacturer's catalogue designated to SKF Group [24]. The bearing selected for point B was single row deep groove ball bearing number: 6302 with inner diameter 15mm, outer diameter 42mm, axial width 13mm, dynamic load carrying capacity of 11400N and static load carrying capacity of 5400N.

Also, at point C, single row deep groove ball bearing number 6002 with inner diameter 15mm, outer diameter 32mm, axial width 9mm, dynamic load carrying capacity of 5590N and static load carrying capacity of 2500N was selected from the manufacturer's catalogue. Consequently, Considering the selected shaft diameter of 20mm, and the various dynamic loads computed in Figure 11, the bearing selection were obtained from manufacturer's catalogue designated for SKF Group [24]. The bearing selected for point B is single row deep groove ball bearing number: 164000 with inner diameter 20mm, outer diameter of 42mm, axial width of 8mm, dynamic load carrying capacity of 7020N and static load carrying capacity of 3400N.

Similarly for point C, a single row deep groove ball bearing number: 6204 with inner diameter of 20mm, outer diameter of 47mm, axial width of 14mm, dynamic load carrying capacity of 12700N and static load carrying capacity of 6200N.finally, following the shaft diameter of d=20mm, alongside with the various calculated dynamic load values computed in Figure 12, the bearing selection were obtained from manufacturer's catalogue designated for SKF Group [24]. The bearing selected for point B is a single row deep groove ball bearing number 6204 with inner diameter 20mm, outer diameter 47mm, axial width 14mm, dynamic load carrying capacity of 12700N and static load carrying capacity of 6200N.

Then, the bearing selected for point C was a single

row deep groove ball bearing number: 61804 with inner diameter 20mm, outer diameter 32mm, axial width 7mm, dynamic load carrying capacity 2700N and static load carrying capacity of 1500N.

Simulation result on conveyor/mixing shaft and frame stability checks.

Simulations conducted on conveyor/mixing shaft to ascertain its stability by analyzing the finite elements is represented in Figure13. The simulation results of upper bound axial and bending stress on the frame is also presented as Figure14.

Figure 13 showed the result of the applied Von Mises stress on the conveyor/mixing shaft. It was observed from Figure 13 that the stated stress decreases in the conveyance direction. The maximum Von Mises stress of 1.847E+00N/mm^2 was obtained at node 10227 that was situated closer to the fixed geometry. Whereas, the minimum Von Mises stress of 1.604E-08N/mm^2 was obtained at node 3312 that was farthest from the fixed geometry. This may be as a result of the fact that the impact of stress is always greater at the point where there is existence of greatest resistance. Judging the stability of the conveyor/mixing shaft based on Von Mises failure criterion, the shaft will not fail, so long as the maximum Von Mises stress on the shaft of 1.847E+00N/mm^2 was far below the material's yield strength of value 2.068E+02N/mm^2.

Figure 14 showed the result of upper bound axial and bending stress at different elements of the frame. The
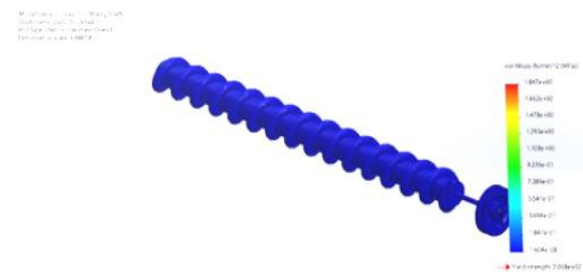

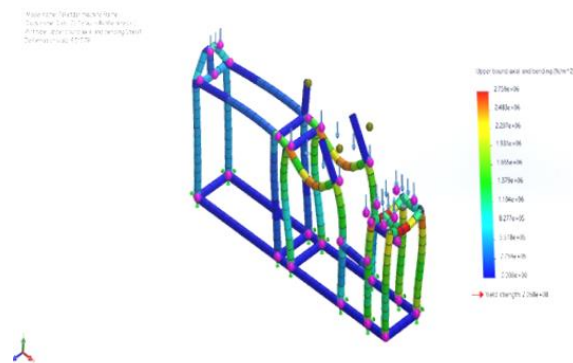**Figure 13.** Von Mises stress on the conveyor/mixing shaft

Figure 14. Upper pound axial and bending stress on the frame

minimum upper bound axial and bending stress of $0.000E+00N/m^2$ was obtained at the element 1 which was indicated with blue colour. Whereas, the maximum upper bound axial and bending stress of $2.759E+06N/m^2$ was obtained at element 100 that supported the motor that drive the entire mechanism. Its position was indicated with red colour. The element receives the highest bending stress due to the impact of the turning torque and moment that drive the entire mechanism alongside with the larger weight of the motor. The failure theories justified the stability of the frame as the maximum upper bound axial bending stress value of $2.759E+06N/m^2$ is far below the materials yield strength of $2.068E+08N/m^2$.

After all the computations that accompanied the design, the broken out isometric view of the expected technology is shown in Figure 15.

Novelty and contribution of the work
This technology was designed in consideration of the prevailing level of technology within the concerned region, detected pelletization gap and the carrier material involved. The work presented alternative technique that could produce uniform shaped homogenous pellets as against either the predominant extrusion methods that release irregular shaped heterogeneous products or more sophisticated balling technologies that created operation related difficulties.
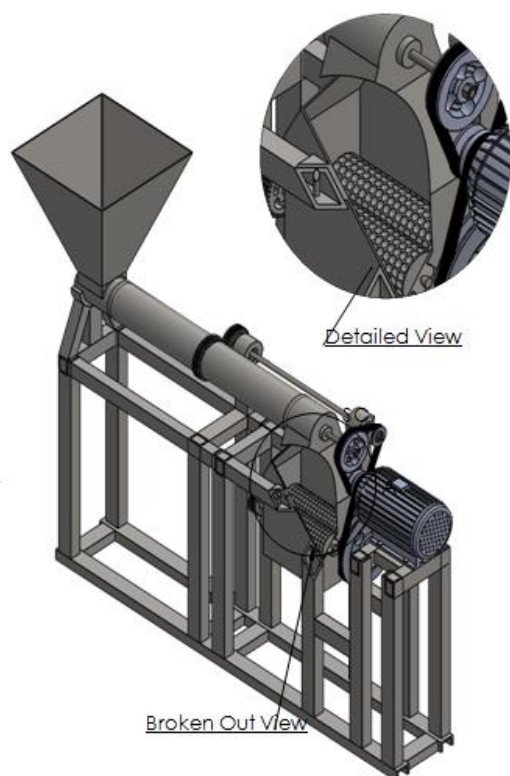

Figure 15. Broken out isometric view of the pelletizer

Bio fertilizer is a renewable source of plant nutrient that heal the land of chemical anomalies resulting from uncontrolled usage of chemical fertilizers. Essence of bio-fertilizer pelletization is to settle it prevalent segregation from the conventional chemical fertilizer to initiate demands for easier applications to the farm. The design thereby provided faster and more reliable alternative that produce pellets by compressing the filled complementary cavities under pressure and release the product consecutively.

CONCLUSION

Rolling process pelletizer was designed to provide a better pelletizing alternative. The machine was designed after considering the dynamics of the various machine elements. The forces and tensions acting on the machine parts were calculated along with the determination of shear forces and bending moments on the shafts. Bearings were selected from SKF bearing catalogue after due considerations. The machine was designed to operate based on the power transmitted from the motor to the various shafts through the belt and pulley arrangements.

Stability simulation test on conveyor/mixing shaft of the designed rolling process pelletizer, passed failure test by resulting into maximum Von Mises stress of $1.847E+00N/mm^2$ that was far below the material's yield strength of $2.068E+02N/mm^2$. Also frame analysis confirmed stability as the upper bound axial and bending stress of $2.759E+06N/m^2$ was below the material's yield strength of $2.068E+08N/m^2$.

Subsequently, the expected bio fertilizer would now be prepared and put in an expected pelletized shape through the designed rolling process pelletizer. A design that incorporated an improved mixing technique of combined rotary mixing and screw mixing technology with stable frame.

REFERENCES

1. Mishra, P. and Dash, D., 2014. Rejuvenation of biofertilizer for sustainable agriculture and economic development, *Consilience,* (11), pp. 41-61. URL: https://core.ac.uk/download/pdf/161452834.pdf

2. Naher, U. A., Ahmed, M., Sarkar, M. I. U., Biswas, J. C. and Panhwar, Q. A., 2019. Fertilizer management strategies for sustainable rice production, *Organic farming*, Elsevier, pp. 251-267. Doi:10.1016/B978-0-12-813272-2.00009-4

3. Zambrano-Mendoza, J. L., Sangoquiza-Caiza, C. A., Campaña-Cruz, D. F. and Yánez-Guzmán, C. F., 2021. Use of Biofertilizers in Agricultural Production, *Technology in Agriculture*, pp. 193. Doi:10.5772/intechopen.98264

4. Chaudhary, P., Jain, D., Anand, K. and Mitra, D., 2019. Biofertilizers: A sustainable approach for plant and soil health, *Microbial Resources for Sustainable Agriculture. LAP LAMBERT Academic Publishing*, pp. 106-119.

5. Jehangir, I., Mir, M., Bhat, M. and Ahangar, M., 2017. Biofertilizers an approach to sustainability in agriculture: a review, I*nternational Journal of Pure and Applied Bioscience,* 5, pp. 327-334. Doi:10.18782/2320-7051.5011

6. Riaz, U., Mehdi, S. M., Iqbal, S., Khalid, H. I., Qadir, A. A., Anum, W., Ahmad, M. and Murtaza, G., 2020. Bio-fertilizers: eco-friendly approach for plant and soil environment, *Bioremediation and Biotechnology*: Springer, pp. 189-213. Doi:10.1007/978-3-030-35691-0_9

7. Audu, I. G., Barde, A., Yila, O. M., Onwualu, P. A. and Lawal, B. M., 2020. Exploring biogas and biofertilizer production from abattoir wastes in Nigeria using a multi-criteria assessment approach, *Recycling,* 5(3), pp. 18. Doi:10.3390/recycling5030018

8. Herrmann, L. and Lesueur, D., 2013. Challenges of formulation and quality of biofertilizers for successful inoculation, *Applied Microbiology and Biotechnology,* 97(20), pp. 8859-8873. Doi: 10.1007/s00253-013-5228-8

9. Oduntan, O., Koya, O. A. and Faborode, M., 2014. Design, fabrication and testing of a cassava pelletizer, *Research in Agricultural Engineering,* 60(4), pp. 148-154. Doi:10.17221/77/2012-RAE

10. Aremu, A., Kadiri, A. and Ogunlade, C., 2014. Development and testing of screw type kenaf (Hibiscus cannabinus) pelletizing machine, *Journal of Agricultural Technology,* 10(4), pp. 803-815.

11. Daniyan, I, Omokhuale, A., Aderoba, A., Ikumapayi, O. and Adaramola, B., 2017. Development and performance evaluation of organic fertilizer machinery, *Cogent Engineering,* 4(1), pp. 1364044. Doi:10.1080/23311916.2017.1364044

12. Daniyan, I. A. and Akhere, O. M., 2017. Development of a Multi Feed Pelletizer for the Production of Organic Fertilizer, *American Journal of Mechanical and Materials Engineering,* 1(2), pp. 44-48. Doi:10.11648/j.ajmme.20170102.13

13. Pocius, A., Jotautiene, E., Zvicevicius, E. and Savickiene, S., 2017. Investigation of effects of organic fertilizer pellet rheological and geometric properties on mechanical strength, 16th International Scientific Conference Engineering for Rural Development, pp. 24-26, Doi:10.22616/ERDev2017.16.N339

14. Vijayaraghavan, G., K. and Vishnupriyan, S., 2015. *Design of machine elements* Chennai, India: LAKSHMI PUBLICATIONS. Available at:

15. Okoli, I. G. and Okonkwo, U. C., 2021. Design of an Improved Double Barrel Cassava Grating Machine, *International Journal of Engineering Research & Technology (IJERT),* 10(12), pp. 112-117.

16. Engineers edge, 2020. *Two pulley connecting belt design and calculations*: Mechanics and machine calculations. Available at: https://engineersedge.com/mechanics_machines/two_pulley_connecting_belt_design_and_calculations_10226.htm.

17. Engineers edge, 2020. *Gear design equation and formula*: ANSI Screw Slide Chart Design Data. Available at: https://engineersedge.com/gear_formula.htm.

18. Kovacevic, A. 2020. Mechanical elements-shafts. ME 1110-Engineering Practice 1, pp. 1-4. Available at: https://Staff.city.ac.uk/~ra600/ME1105/Handouts/ME1110-15-H.pdf

19. Gao, H., 2014. The Theory of Materials Failure, *Materials Today,* 17(2), pp. 94-95. Doi:10.1016/j.mattod.2014.01.016

20. Burns, S. J., 2015. The Theory of Materials Failure, by Richard M. Christensen, *Contemporary Physics,* 56(3), pp. 404-404. Doi:10.1080/00107514.2015.1049209

21. Atikpakpa, A., Okafor, C. E. and Ugo, O., 2016. Failure and reliability evaluation of turbines used in Nigerian thermal plant, *Journal of Science, Technology and Environment Informatics,* 4(01), pp. 280-292. Doi:10.18801/jstei.040116.31

22. Sengupta, 2019. Working stress and failure theories: A simplified approach *MET 301:Theories of failure*, pp. 1-9.

23. Atiyah, A., A., 2019. *Failure theories* Iraq: Department of Materials Engineering, University of Technology. Available at: https://researchgate.net/publication/332397228_failure_theories (Accessed: Retrieved on March 11, 2020).

24. Group, S., 2018. *Ball bearing and cylindrical product data, Rolling bearings (239-516)*

25. Okonkwo, U. C., Okafor, C. E. and Ihueze, C., 2020. Development and Performance Evaluation of a Double Barrel Cassava Grating Machine, *SSRN 3803810.* Doi:10.47752/sjsr.311.133.140

https://www.researchgate.net/publication/328926726_Design_of _Machine_Elements.

Persian Abstract

چکیده

گندله‌ساز فرآیند نورد که تکنیک گلوله‌سازی کارآمدتری را ارائه می‌دهد و تولید کودهای زیستی را آسان می‌کند، طراحی شد. مکانیسم‌های طراحی‌شده بر روی دینامیک اجزای ماشین متمرکز گردید که عمدتاً از پیوندها و اتصالات تشکیل شده‌اند. تنش‌ها و بارها با پیروی از معادلات موازنه نیرو تعیین شدند. یاتاقان‌ها از کاتالوگ بلبرینگ SKF با در نظر گرفتن موقعیت آنها، ارزیابی نیازهای تئوری‌های شکست در کنار ظرفیت‌های حمل بار دینامیکی انتخاب شدند. آزمایش پایداری بر روی نوار نقاله/میکس‌کننده با جرم ۱۱/۲۵۶۱ کیلوگرم و چگالی ۸۰۰۰ کیلوگرم بر مترمکعب با تثبیت یک انتها و اعمال فشار ۱۰-۱۰-۱/۱۰۶۱ نیوتن بر میلی‌متر مربع به سمت انتهای دیگر مطابق با خواسته‌های نظریه انرژی اعوجاج انجام شد. تست پایداری قاب نیز با اعمال مش پرتویی انجام شد که ۳۵۴ گره و ۳۳۴ عنصر تولید کرد. کشش ۲۰۵/۲ N و ۱۲۶/۵ N در قرقره محاسبه شد. بارها و ممان‌های مختلفی که بر روی شفت‌های مختلف اثر می‌کنند، تعیین و به صورت نموداری نمایش داده شد. فون از تنش ۱/۸۴۷ E+00N/mm² روی شفت نوار نقاله و تنش محوری و خمشی کران فوقانی ۲/۷۵۹ E+06N/m² روی قاب که کمتر از مقاومت تسلیم ماده ۲/۰۶۸ E+08N/m² بود طبق آزمون شبیه‌سازی، پایداری طرح را نشان داد. انتظار می‌رود این طرح در مناطق تولید مشابه نیز عمل کند.